Journal of Aircraft, Vol. 55, Issue 3, 2018, pp. 905-917
DOI:10.2514/1.C033132

Multiobjective Environmental Departure Procedure Optimisation

Quintain McEnteggart* and James F. Whidborne†
Cranfield University, Bedfordshire, England MK43 0AL, United Kingdom

Abstract

To achieve a sustainable future for air transport, the International Civil Aviation Organization has proposed goals for reductions in community noise impact, local air quality and climate impacting emissions. The paper focuses on the contribution aircraft operations make to those goals. It describes a multiobjective optimisation methodology intended to support the planning of environmentally efficient departure procedures. The methodology treats the problem as a multiobjective optimal control problem that is solved through the application of a direct method of trajectory optimisation and a multiobjective version of the Differential Evolution algorithm. The method generates Pareto fronts between several competing objectives allowing the decision maker to make informed decisions about potential trade-offs between different environmental goals. The methodology is demonstrated through its application to a real world many objective procedure optimisation study. The method supported in depth analysis of the problem not achievable through existing methods and was used to identify a solutions set that offered improvements in all environmental objectives relative to the existing procedure design.

*Research Student, Dynamics, Simulation and Controls Group
†Ph.D., Reader, Dynamics, Simulation and Controls Group

Nomenclature

C	=	scale factor
CO,HC,NOx	=	carbon, hydrocarbons, oxides of nitrogen
$CO2,H20,SOx$	=	carbon dioxide, water vapor, sulphur oxides
CR	=	crossover constant
$d_{k_{NN}}$	=	k nearest neighbour crowding distance
g	=	gravitational acceleration
J	=	objective functional
k	=	number of optimization objectives
L_p, L_A	=	sound level, A weighted sound level
L_{AeqT}	=	equivalent noise level
m	=	aircraft mass
n	=	load factor
p	=	pressure
$r_{1,2,3}$	=	Cartesian coordinates
T,L,D	=	thrust, lift, drag forces
t,X,U	=	time, state and control variables
v	=	velocity
W	=	fuel flow
w_x,w_y,w_z	=	wind speed components
x,y,z	=	position states
$\bar{\mathbf{v}}, \bar{\mathbf{x}}, \bar{\mathbf{u}}$	=	mutant, target and trial parameter vectors
γ, χ, ϕ	=	flight-path, heading and roll angles
λ	=	speed factor
τ	=	virtual arc
$(.)', (.)'', (.)'''$	=	derivatives with respect to τ
$\dot{(.)}$, $\ddot{(.)}$, $\dddot{(.)}$	=	derivatives with respect to time

1 Introduction

Over the last decade global passenger air traffic has increased by more than 45% , with continued high levels of growth projected for the coming decade [1]. This growth however has come with an environmental cost. Increasing traffic levels and the greater consumption of fossil fuels have led to increased emissions of climate changing gases and particulate matter impacting local air quality. Increasing traffic levels have also, despite an increasingly quiet aircraft fleet, led to an increase in the number of people exposed to significant levels of aircraft noise [2].

To achieve a sustainable future for air transport, the International Civil Aviation Organization (ICAO) has proposed 3 high level environmental goals for international aviation [2]:

i) to limit or reduce the number of people affected by significant aircraft noise,

ii) to limit or reduce the impact of aircraft engine emissions on local air quality,

iii) to limit or reduce the impact of aviation greenhouse gas emissions on the global climate.

In Europe, the current ICAO environmental goals are complemented by strategic industry goals of continuing reductions in aviation environmental impact [3–5].

While approaching and departing the terminal area, aircraft are constrained to fly along procedural routes developed by Air Navigation Service Providers (ANSP). The routes termed Standard Instrument Departures (SIDs) and Standard Arrival Routes (STARs) serve a number roles. They provide obstacle avoidance and navigational support to aircraft departing and arriving to airports. They also support the safe management of traffic by creating corridors of traffic that can be easily managed by air traffic control. Of increasing importance is the environmental design of the routes and how the horizontal placement of the route and the aircraft vertical profile along the route can be optimised for environmental impact.

1.1 Trajectory Optimization

The environmental optimization of arrival and departure routes and operating procedures fall under the broad category of green trajectories. The Continuous Descent Approach (CDA) is an operating procedure for aircraft descents. The CDA ideally involves the aircraft descending from cruise to the runway while eliminating or minimising level approach segments, minimising thrust settings and maintaining a low drag configuration for as much of the descent as possible. In recent years the CDA trajectory has been studied in detail [6]. CDAs can be implemented with current day technology levels and hence require relatively low investment costs. CDA procedures have been implemented at a number of major airports as they offer reductions in community noise impact as well as reductions in fuel consumption leading to lower emissions and lower airline operating costs [7].

The ICAO Procedures for Air Navigation Services - Aircraft Operations (PAN-OPS) document [8] contains recommended departure flight procedures that are complementary to CDAs and aim to reduce aircraft noise impact on departure. The PAN-OPS procedures, termed Noise Abatement DeParture climbs (NADP) 1 and 2 are aircraft operating procedures that can be applied to any departure routing. NADP 1 is designed to minimise noise near to the airport and NDAP 2 is designed to minimise noise further out from the airport. Further to the PAN-OPS guidance, the Sourdine project [9] used expert analysis to develop noise optimised take-off procedures for a representative medium narrow-body and large wide-body aircraft. The PAN-OPS and Sourdine recommended flight procedures offer general guidance on minimising departure noise impact. However, neither set of recommended procedures are optimised to local conditions, and may require significant modification to fully realise potential noise benefits.

To account for this Visser [10] [11], treating the problem as an optimal control problem, used a direct collocation method [12], noise mapping software and a Geographic Information System (GIS) database to define 3D noise abatement procedures that minimise sleep disturbance related to aircraft noise at communities surrounding Amsterdam Airport Schiphol. Hebly [13] extended this approach by including an aircraft emissions model and comparing the results of optimising an RNAV SID for emissions relative to optimising for

awakenings from aircraft noise. Similarly, Houacine [14] used a Gauss Pseudospectral collocation method to compare the differences between trajectories optimised for noise levels under the aircraft centreline and for fuel consumption. Soler [15], extending the problem beyond individual climbs and descents, used a direct collocation approach [12, 16] to calculate a minimum fuel consumption trajectory for a multiphase climb, cruise and descent problem.

It has been shown in an ICAO study of noise abatement procedures [17], particularly for departure operations, that there are multiple trade-offs to be made among various noise objectives and also between noise and emissions objectives. Prats [18] tackled the multi-objective nature of the environmental objectives by treating the problem as an multi-objective optimal control problem. The problem was then solved with a direct collocation method and a lexicographic based optimisation technique. The lexicographic method required the definition of a hierarchy of objectives. The approach then uses a series of single objective optimisations, first finding the minimum of the objective highest in the hierarchy, before moving on to minimise objectives lower in the hierarchy, adding constraints at each optimisation step to preserve the higher ranked objectives. The lexicographic method produces a single Pareto optimal point and requires the definition of the importance of each objective prior to the optimization.

In many cases, the decision maker finds it desirable to be informed about the full range of trade-off options in order to choose the solutions that provide the best balance between the objectives. In this case, the Pareto optimal set is desirable. The solution vector $\mathbf{s}^*$ of a multi-objective optimisation problem is Pareto optimal, if there is no other solution vector $\mathbf{s} \in S$ where $s_i \leq s_i^*$ for all objectives $i = \{1, \ldots, k\}$ and where $s_j^* < s_j$ for at least one index j, $j \in \{1, \ldots, k\}$. A Pareto front is a set of Pareto optimal solutions. The Pareto optimal set identifies the extrema of the objectives and allows trade-offs between the objectives to be quantified and visualised. This is especially useful to decision makers trying to balance conflicting objectives. The set represents the best available trade-offs between different objectives.

Pervier et al [19] and Torres et al [20] treated the problem of calculating Pareto optimal fronts between environmental objectives as a discrete parameter optimization problem with bounded variables to maintain feasibility. However, the search for the Pareto front can be treated as an multiobjective optimal control problem. Here, the cost functionals take as their input a set of functions representing the states and controls of the aircraft. Optimal control problems have infinite dimensions. Generally, to solve an optimal control problem, the infinite dimensional problem must be converted to a finite dimensional problem that can be solved with standard numerical methods.

Currently there is no methodology that can be used alongside the three ICAO environmental goals to identify trade-offs in procedures optimised for several conflicting environmental objectives. Therefore there is a need for an approach that can be used to manage the trade-offs in an informed manner. This paper proposes such a methodology. The method uses current best practice environmental cost models and treats the problem as a multi-objective optimal control problem. The problem is then solved for a set of Pareto optimal solutions by discretising the optimal control problem with a direct numerical method and solving the resulting Non Linear Programming (NLP) problem with the stochastic Differential Evolution solver. The method is applied to a real world environmental procedure optimization case study to determine if the proposed method could identify procedures that provided better trade-offs between the environmental impacts than those proposed in the initial study.

2 Multiobjective Optimal Control Problem

The multi-objective optimal control problem can be stated as a problem of minimising an array of single objective functionals

$$\begin{aligned} &\min_{\mathbf{X}\in X,\mathbf{U}\in U}[J_1, J_2, \ldots, J_k]^T \\ \text{subject to } &\dot{\mathbf{X}} = \mathbf{f}(\mathbf{X}, \mathbf{U}, t) \\ &\mathbf{X}(0) = \mathbf{X}_0 \\ &\mathbf{\Psi}(\mathbf{U}_f, \mathbf{X}_f) \leq 0 \end{aligned} \tag{1}$$

where k is the number of objectives, $\mathbf{X}(t) \in \mathbb{R}^n$ is a vector of state trajectories, $\mathbf{U}(t) \in \mathbb{R}^m$ is a vector of control trajectories and the system dynamics are described by a set of ordinary differential equations $\dot{\mathbf{X}} = \mathbf{f}(\mathbf{X}, \mathbf{U}, t)$. The system must satisfy some initial condition given by $\mathbf{X}(0) = \mathbf{X}_0$, and there is some terminal constraint $\mathbf{\Psi}(\mathbf{U}_f, \mathbf{X}_f) \leq 0$ where t_f is the final time. The individual objectives are then

$$J_i = \int_{t_0}^{t_f} f_i(\mathbf{X}(t), \mathbf{U}(t), t)dt + \phi_i(\mathbf{X}_f, t_f), \quad i = 1, \ldots, k, \tag{2}$$

2.1 Numerical Methods

Betts categorised the two approaches for solving optimal control problems as direct and indirect methods. For indirect methods the problem is converted to a two point boundary value problem and numerical methods are used to find the root of the problem. For direct methods, the states and/or controls in the optimal control problem are parameterised using polynomial approximations to the functions. The optimal control problem is then transcribed to a NLP problem by discretising the polynomial interpolations and solving for the states and controls at each of the dividing nodes. Direct methods were considered appropriate for this work due to their good convergence properties and ease of application to the multi-objective problem. Direct methods considered for application were the inverse dynamics method and direct collocation methods.

For collocation methods, both the states and controls are parameterised. The state and controls at the nodes are the optimization variables and defect constraints are used to enforce the system dynamics at or between nodes [21]. Collocation schemes exist in two forms, local and global [22]. Local collocation uses piecewise polynomials often derived from numerical integration schemes, where the number of segments is varied to better approximate the functions [12] [23]. Global collocation, such as pseudospectral methods, uses global polynomials, where the degree of the polynomial is varied. Global polynomials can be used with several different forms of collocation points impacting interpolation speed and accuracy [24], [25], [26].

Yakimenko [27] proposed an inverse method where the position states of the aircraft and their derivatives are parameterised using 7th degree polynomials. Controls are then determined by inverting the state equations. The method significantly reduces the number of optimization variables required by analytically determining the polynomial coefficients from the prescribed states and controls at the boundaries ($t = 0$ and $t = t_f$). Instead of parameterising by time, Yakimenko adopted Taranenko's method [28] of parameterising the polynomials by τ, creating a virtual arc $\tau \in [0, t_f]$. The relationship between time t and τ is defined as $\lambda = d\tau/dt$. The use of the relationship parameter τ allows the definition of aircraft velocity using a separate reference function, enabling the creation of a virtual speed profile along the trajectory path of the aircraft [29]. The method, termed the Inverse Dynamics in the Virtual Domain (IDVD) method, is a fast trajectory optimization method and has been considered for real time implementation [30].

The IDVD method was favoured for this work due its compatibility the multi-objective Differential Evolution (DE) NLP solver chosen for this work. DE uses a computationally intensive trial and error approach to finding the Pareto front. Collocation schemes, which have large numbers of optimization parameters act to further increase the computational complexity of the problem. The inverse method on the other hand, when applied with a three Degree of Freedom (DOF) aircraft dynamics model, results in a system with six aircraft states, three controls and nine optimization variables. This allows the combination of the IDVD and DE methods to quickly progress solutions from infeasible to feasible to a point on the global Pareto front. The

principle drawback of the approach is the accuracy offered by the global interpolating polynomials, which are only of degree seven. This is considerably fewer than what may be available from adopting collocation schemes. However, as commercial aircraft have relatively unaggressive trajectories and as the environmental models adopted are sensitive to macro rather than micro changes in the trajectory, the low parameter space offered by the IDVD method was considered more beneficial than the higher fidelity potentially offered by collocation schemes.

3 Inverse Dynamics

The key idea of the inverse dynamics method is to parameterise a set of output trajectories that fully define all states and inputs in terms of those outputs and their derivatives. The state and control vectors are expressed as functions of the output trajectory vector $\mathbf{r} = [r_1(t), r_2(t), r_3(t)]$ and its derivatives, where $r_1(t), r_2(t), r_3(t)$ are the Cartesian x, y, z coordinates $\forall t \in [t_0, t_f]$. Yakimenko recommended parameterising the flat earth Cartesian coordinates and their derivatives using 7th order polynomials, where the trajectory is generated in the output space and the input controls and the remaining states are then determined algebraically.

For the inverse method, the Cartesian positional states $r_j \ \ (j = 1, 2, 3)$ of the aircraft and their derivatives are parameterised by the folllowing reference function and its derivatives:

$$r(\tau)_j = \sum_{i=0}^{7} \frac{a_j i \tau^i}{\max(1, i(i-1))} \tag{3}$$

For the virtual arc, derivatives of $(\cdot)$ with respect to τ are denoted $(\cdot)', (\cdot)'', etc.$ Time derivatives are denoted as $\dot{(\cdot)}, \ddot{(\cdot)}, etc.$ The coefficients of the reference polynomials defined by (3) are determined analytically from the coordinates and their derivatives at the boundaries ($\tau = 0$ and $\tau = \tau_f$) by making the coefficients the subjects of the following set of linear equations

$$\begin{bmatrix} 1 & 0 & 0 & 0 & 0 & 0 & 0 & 0 \\ 0 & 1 & 0 & 0 & 0 & 0 & 0 & 0 \\ 0 & 0 & 1 & 0 & 0 & 0 & 0 & 0 \\ 0 & 0 & 0 & 1 & 0 & 0 & 0 & 0 \\ 1 & \tau_f & \tau_f^2/2 & \tau_f^3/6 & \tau_f^4/12 & \tau_f^5/20 & \tau_f^6/30 & \tau_f^7/42 \\ 0 & 1 & \tau_f & \tau_f^2/2 & \tau_f^3/3 & \tau_f^4/4 & \tau_f^5/5 & \tau_f^6/6 \\ 0 & 0 & 1 & \tau_f & \tau_f^2 & \tau_f^3 & \tau_f^4 & \tau_f^5 \\ 0 & 0 & 0 & 1 & 2\tau & 3\tau^2 & 4\tau^3 & 5\tau^4 \end{bmatrix} \begin{bmatrix} a_{j0} \\ a_{j1} \\ a_{j2} \\ a_{j3} \\ a_{j4} \\ a_{j5} \\ a_{j6} \\ a_{j7} \end{bmatrix} = \begin{bmatrix} r_{j0} \\ r'_{j0} \\ r''_{j0} \\ r'''_{j0} \\ r_{jf} \\ r'_{jf} \\ r''_{jf} \\ r'''_{jf} \end{bmatrix} \tag{4}$$

A defining feature of the inverse method is the parametisation of the polynomials over the virtual arc τ. Parameterising by time explicitly links the path and speed profile along the path. Parameterising by τ allows the path optimization to be separated from the speed profile. The speed profile may then be predetermined or alternatively defined by a separate reference function (3). Parameterising the speed profile in this manner adds an extra degree of freedom to the optimization that allows the speed profile to be optimized along the trajectory path of the aircraft. The relationship between the parameterised speed v and the speed along the virtual arc $\sqrt{x'^2 + y'^2 + h'^2}$ is then defined as

$$v = \lambda \sqrt{x'^2 + y'^2 + h'^2} \tag{5}$$

where λ is the scale or speed factor. It follows then that

$$\lambda = \frac{v}{\sqrt{x'^2 + y'^2 + h'^2}} \tag{6}$$

The virtual arc is discretised by nodes $j = 1 \ldots N$ where the N is the number of nodes. Where values are assessed at each node, the parameterised speed is greater than then virtual arc speed when $\lambda_j > 1$. The virtual arc speed is less than v_j when $\lambda_j < 1$, and both the speed profiles are identical where $\lambda_j = 1$. The

optimization variables are then the aircraft initial and final jerks and τ_f such that the optimization vector is $\Xi = [x'''_{0,f}, y'''_{0,f}, h'''_{0,f}, v''_{0,f}, \tau_f]$. Conversion between the time and arc derivatives is achieved by

$$\begin{aligned} \dot{r} &= \lambda r'; \quad \ddot{r} = \lambda(r''\lambda + r'\lambda') \\ \dddot{r} &= \lambda^3 r''' + 3\lambda^2\lambda' r'' + (\lambda^2 + \lambda\lambda'^2)r' \end{aligned} \tag{7}$$

To transform the polynomials to the system dynamics, a point mass model is used. Therefore the states and controls are determined by inverting the following equations, where the drag is modelled using the BADA drag polars [31]. Aircraft mass is m, g is gravitational acceleration and n is the load factor. The wind speed in the 3 coordinate directions is $[w_x, w_y, w_z]$. As in [32], the wind's impact on velocity and path are considered but not its impact on acceleration. The point mass model is given by

$$\begin{aligned} \dot{x} &= v\cos\gamma\cos\chi - w_x, & \dot{v} &= \frac{T-D}{m} - g\sin\gamma \\ \dot{y} &= v\sin\chi\cos\gamma - w_y, & \dot{\chi} &= \frac{gn\sin\phi}{V\cos\gamma} \\ \dot{h} &= v\sin\gamma - w_z, & \dot{\gamma} &= \frac{g}{V}(n\cos\phi - \cos\gamma) \end{aligned} \tag{8}$$

Once the states and control histories are determined from τ_o to τ_f, constraints are applied to ensure that they lie between defined limits determined from the BADA database:

$$\begin{aligned} x &\in [x_{min}, x_{max}] & y &\in [y_{min}, y_{max}] & h &\in [h_{min}, h_{max}] \\ T &\in [T_{max}; T_{min}] & n &\in [n_{max}; n_{min}] & |\phi| &\leq |\phi_{max}| \\ v_{CAS} &\in [v_{max,CAS}; 1.2v_{stall,CAS}] & v &\in [v_{max}; v_{min}] & |a_l| &\leq |a_{l_{max}}| \\ |a_n| &\leq |a_{n_{max}}| & \gamma &\in [\gamma_{max}; \gamma_{min}] & \chi &\in [\chi_{max}; \gamma_{min}] \end{aligned} \tag{9}$$

where the longitudinal acceleration is $a_l = \dot{v}$ and the normal acceleration is $a_n = \dot{\gamma}v$. Therefore, the state and control vectors are expressed as functions of the output trajectory vector $\mathbf{r}$ and its derivatives such that

$$\mathbf{X} = \mathbf{f}_X(\mathbf{r}, \dot{\mathbf{r}}, \ddot{\mathbf{r}} \ldots) \qquad \mathbf{U} = \mathbf{f}_U(\mathbf{r}, \dot{\mathbf{r}}, \ddot{\mathbf{r}} \ldots) \tag{10}$$

This allows the optimal control problem to be converted to a NLP problem where the trajectory search is conducted in the output space and only the algebraic equations need to be solved.

4 Environmental Metrics

Noise is defined as unwanted sound perceived as disturbing or even painful [33]. Single event noise metrics assess the noise emitted during one specific event. A single event is a single aircraft operation, such as a departure, arrival or over-flight. The extent of the unacceptability of the noise depends on the physical characteristics of the sound, notably its intensity, duration and frequency. A number of metrics have evolved to capture one or more of these physical characteristics. Single event metrics commonly used to examine aircraft noise are L_{Amax} and the Sound Exposure LeveL (SEL) [33]. L_{Amax} and SEL are derived from the Sound Pressure Level (SPL) metric.

The Sound Pressure Level

Sound is caused by changes in air pressure. The SPL (SPL or L_p) is the difference in sound pressure from a reference level caused by a sound wave. SPL is the base metric used for constructing single event noise metrics. The SPL is a function of the logarithmic ratio between the measured Root Mean Squared (RMS) sound pressure p_{RMS} and a reference sound pressure p_{ref}, both measured in Pascals (Pa). The units of the

SPL are decibels, and the logarithmic nature of the metric allows the metric to capture the sensitivity of the human ear to a wide range of sound intensities. The SPL is calculated as

$$L_p = 10 \log_{10} \left(\frac{p_{RMS}^2}{p_{ref}^2} \right) \tag{11}$$

with the root mean square pressure p_{RMS}^2 calculated from

$$p_{RMS}^2 = \frac{1}{t_2 - t_1} \int_{t_1}^{t_2} p(t)^2 dt \tag{12}$$

where t_1 and t_2 are the start and end times of the sound event and p is pressure in Pascals. The reference pressure p_{ref} is then

$$p_{ref} = 20 \cdot 10^{-6} \tag{13}$$

L_{Amax}

To better correlate sound levels to perceived sound, the SPL (L_p) is weighted with respect to loudness to produce the A-weighted SPL (L_A) measured in A-weighted decibels (dBA). The maximum A-weighted sound pressure level for a noise event during a specific time interval is then the L_{Amax} (dBA).

SEL

The Sound Exposure Level (SEL), measured in dBA, considers both the loudness and the duration of the noise event above a low cut off point of $L_{Amax} - 10dB$. The total noise energy for the event is then normalised to reference time t_{ref} of 1 second. The SEL is calculated as

$$SEL = 10 \log_{10} \left(\frac{1}{t_{ref}} \int_{t_1}^{t_2} 10^{\frac{L_A(t)}{10}} dt \right) \tag{14}$$

where t_1 to t_2 is the duration of the noise event above the cut-off limit.

Noise Annoyance Score

The Noise Annoyance Score, developed as part of the MIME study [34], is a single event noise metric that attempts to include consideration of the annoyance experienced by populations overflown. The Annoyance Score was developed from the Equivalent Noise Level (LEQ) metric by considering the relationship between the SEL measure and LEQ. LEQ (15) is a long term noise metric that is used with dose response functions to describe the relationship between noise levels and community annoyance [33]. The discrete form of LEQ involves the sum of SELs from multiple single events averaged over a specific time period such as 1 day. LEQ is calculated as

$$L_{AeqT} = 10 \log_{10} \left(\frac{1}{t_{ref}} \sum_i 10^{\frac{SEL_i}{10}} \right) \tag{15}$$

Granoien et al [35], noting the relationship between LEQ and annoyance that exists for multiple events, proposed that each event makes a contribution to the total annoyance. Therefore, in [35] it was proposed that the annoyance experienced at a single point from a single event is proportional to the anti-log of the SEL (SE) for that event,

$$\text{Annoyance} \propto 10^{\frac{SEL}{10}} = SE \tag{16}$$

The proposed Annoyance Score is then the linear sum of the SE for each grid cell weighted by the population of that cell (17). Where the cell population is Pop_c and c is the grid cell index,

$$\text{Annoyance Score} = \sum_c Pop_c SE_c \tag{17}$$

The noise Annoyance Score was used in this study alongside L_{Amax} (dBA) to assess community noise impact. In contrast to other noise metrics, it provides a single value that can be used to assess the community noise impact, making it well suited for use in optimization studies.

Noise Modelling

For the calculation of civil aircraft noise impact local to airports, the dominant method used in the field is the Noise Power Distance (NPD) method [36], [37]. The NPD method utilises, for a number of noise metrics, tables of empirical data that relate the noise level calculated on the ground to the power utilised by the aircraft and the distance from the aircraft to the noise assessment point. Specifically, the noise level at a point is calculated as

$$\text{noise level} = f(T(\mathbf{X}, \mathbf{U}, t), d(\mathbf{X}, \mathbf{U}, t), \boldsymbol{\beta}), \ldots \forall t \in [t_o, t_f] \tag{18}$$

where T is thrust, d is slant distance and $\boldsymbol{\beta}$ is a set of segment level correction terms. The variables t_o and t_f are respectively the start and end times of the trajectory. Power, in this instance, is corrected net thrust. The noise model chosen for use in this work is the Integrated Noise Model (INM). INM is a model developed by the Federal Aviation Administration (FAA) to assess the impact of civil aircraft noise on communities local to airports. INM version 7 [37] is fully compatible with ECAC Doc 29 [36] guidance that provides a standardized methodology for the computation of noise contours around civil airports.

Fuel and Emissions

For the calculation of aircraft emissions, the emissions CO2, water vapor (H2O) and sulphur oxides (SOx) are calculated using direct multipliers on fuel burn, such that their rate of emissions is

$$\dot{e}(t) = f_e(W(t), \boldsymbol{\alpha}) \tag{19}$$

where $W(t)$ is the rate of fuel burn and $\boldsymbol{\alpha}$ is a set of fuel burn multipliers. For the work presented in this paper, rate of fuel burn is calculated using the BADA fuel flow model [31], where $W(t)$ is a function of thrust and the thrust specific fuel consumption factor η such that

$$W(t) = f_W(T(t), \eta) \tag{20}$$

The emissions for hydrocarbons (HC), carbon (CO), and oxides of nitrogen (NOx) are calculated using the Boeing Fuel Flow Methodology (BFFM) [38]. The ICAO emissions databank contains empirical information for certified engines that relate fuel burn to emissions indices at 4 different engine thrust settings. The BFFM offers a procedure for correcting the data for atmospheric conditions and for interpolating the data to calculate emissions of HC, CO, and NOx from in-flight fuel flow. The BFFM uses the ICAO indices to create 2 standard type plots. Figure 1 shows the 2 standard Log-Log interpolation plots for fuel burn against the emissions indices of NOx, HC, and CO at sea level static conditions.

For NOx emissions, a least squares linear line is fitted to the 4 emissions database data points, reflecting the linear relationship between fuel burn and NOx. For the emissions HC and CO, a 2 segment plot is created consisting of a diagonal line connected to a flat horizontal line. The diagonal line reflects how emissions of HC and CO decrease with increasing thrust and fuel flows. The inverse relationship between the emissions and fuel flow occurs because of the the more efficient burning of fuel that occurs at high combustion temperatures

related to higher aircraft thrust settings. The connected horizontal lines reflect that there is a point where the reduction in emissions plateaus and that beyond this point there are no further reductions in the emissions for higher levels of fuel flow.

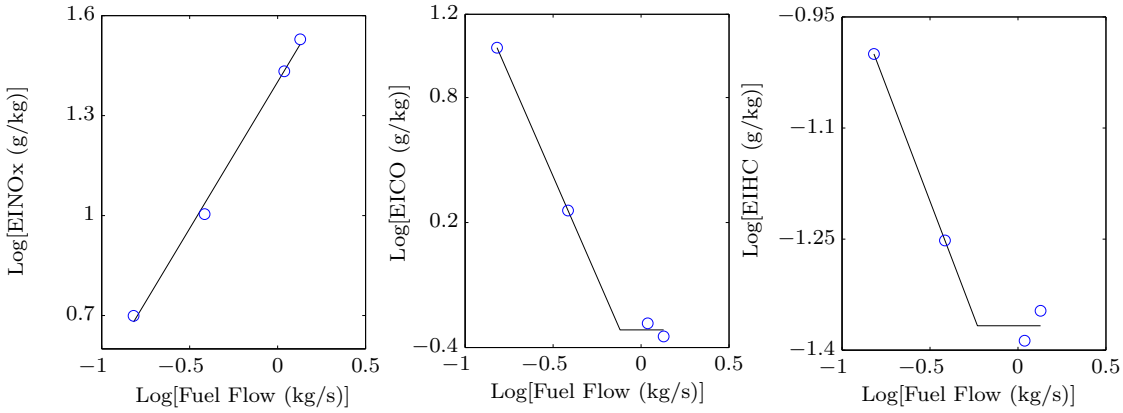

Figure 1: Log-Log plots of fuel burn against emissions indices for a A320/V2530 aircraft

For the BFFM method, in flight fuel flow is corrected to sea level conditions, where the emissions values are interpolated off the Log-Log plots and the results are then corrected back to in-flight conditions. Therefore the rate of NOx, HC and CO emissions is calculated as

$$\dot{e}(t)_{EI} = f_{EI}(W(t), \mathbf{EI}) \tag{21}$$

where **EI** is a set of emissions indices.

5 Differential Evolution

Differential evolution is a simple and effective heuristic for global optimization [39] [40]. As with many evolutionary algorithms, DE creates a randomly generated first parameter population. Elements of the initial population are then combined to form a trial population. The objective values from the initial population are tested against those of the trial population to determine the population members to be carried forward to a further generation. The process of mutation, combination and selection continues until no better objective value can be found.

One of the defining characteristic of DE is the differential mutation mechanism. Differential mutation creates a new mutant parameter vector $\bar{\mathbf{v}}$ by finding the difference between two parameter vectors $\bar{\mathbf{x}}_{r1}$, $\bar{\mathbf{x}}_{r2}$ and adding the scaled difference to a third parameter vector $\bar{\mathbf{x}}_{r3}$. One of the advantages of using difference vectors is that they scale the step size to the objective function surface [40]. The mutation operation is $\bar{\mathbf{v}}_{i,G+1} = \bar{\mathbf{x}}_{r3,G} + C\left(\bar{\mathbf{x}}_{r1,G} - \bar{\mathbf{x}}_{r2,G}\right)$ for $i = 1, \ldots, NP$, where $r1, r2, r3 \in \{1, \ldots, NP\}$ are randomally chosen except that $r_1 \neq r_2 \neq r_3 \neq i$. The scale factor $C \in (0, 1]$ and NP is the number of populations.

The other defining characteristic of DE is the Crossover Constant (CR), which is a value between 0 and 1 that determines how much of the mutant vector $\bar{\mathbf{v}}$ is crossed with the target vector $\bar{\mathbf{x}}$ to form the trial vector $\bar{\mathbf{u}}$. The higher the CR value the more greedy the trial vector becomes for mutant parameters. The crossover operation is described by

$$\bar{u}_{j,i,G+1} = \begin{cases} \bar{v}_{j,i,G+1} & \text{if rnd}_j[0,1) \leq CR \vee j = b \\ \bar{x}_{j,i,G} & \text{otherwise} \end{cases} \tag{22}$$

where $rnd_j[0, 1)$ is a uniform random number generation between 0 and 1, $b \in \{1, \ldots, D\}$ is a randomly chosen index and D is the length of the parameter vector.

DE has been shown to be an effective solver when combined with the IDVD method for single objective trajectory optimization problems. Drury [41] tested the performance of DE and other popular NLP solvers, SNOPT, Nelder Mead and Hook Jeeves with the IDVD method for 2000 different boundary value sets. DE outperformed the other solvers with a robustness of 99.8% and relative optimality score of 94%.

Differential evolution, at each step of an optimization, maintains a population of solutions, allowing the algorithm to simultaneously explore different parts of the solution space. This makes the algorithm well suited for multi-objective optimization. Ranier and Storn proposed a multi-objective method with Pareto dominance selection in [40]. In general, for two feasible solutions where $\mathbf{p}, \mathbf{q} \in S$, $\mathbf{p}$ dominates $\mathbf{q}$ $(\mathbf{p} \prec \mathbf{q})$ if $\forall k : f_k(\mathbf{p}) \leq f_k(\mathbf{q}) \wedge \exists k : f_k(\mathbf{p}) < f_k(\mathbf{q})$. Fonseca and Fleming [42] with their MOGA algorithm and Srinivas and Deb [43] with their NSGA algorithm highlighted the importance of elitism and diversity in finding the Pareto front solution set. Therefore work in [44, 45] proposed supplementing DE's mutation mechanism with selection methods based on nondominated sorting and the crowding distance measure proposed by Deb for the Nondominated Sorting Genetic Algorithm II (NSGAII) [46]. The DEMO (Differential Evolution for Multiobjective Optimization) [47] and GDE3 (Generalized Differential Evolution) [48] methods both supplement nondominated sorting and crowding distance with an additional greedy selection step.

Nondominated sorting uses domination to rank each member of a population and then sorts the population into fronts that are sets of solutions with equal dominance ranking. Population truncation then occurs where the most elite ranking solutions are retained. Where truncation splits a front, the solutions in the front are further sorted by their crowding distance such that the most diverse of the solutions are preserved.

In [49] it is shown that the crowding distance measure proposed by Deb in [46] provides good diversity in the case of two objectives, but does not perform well for objectives of three or more. As highlighted in [17] and [2], the departure procedure optimization is a problem of more than 2 objectives. For problems with many objectives, [50] proposes an improved crowding distance measure. With k being the number of objectives, the measure is based on finding the distance to the kth nearest neighbors, which are multiplied together to determine a crowding distance $d_{k_{NN}}$ calculated as

$$d_{k_{NN}} = \prod_{i=1}^{k} L_2^{NN_i} \tag{23}$$

where $L_2^{NN_i}$ is the distance to the ith nearest neighbor according to the L_2 distance metric.

The pruning algorithm proposed in [50] aims to avoid a brute force approach of calculating the distance from each solution to every other solution and uses pre-calculated projection values to provide a fast way to determine the distances between each solution and its k nearest neighbours.

In the methodology proposed in this paper, the NLP algorithm used adopts the GDE3 mutation and selection mechanism, however the crowding distance measure is calculated using the k nearest neighbour approach proposed in [50].

6 Results

Terminal Control (TC) North is an arrangement of airspace sectors north of London, UK. As part of a planned airspace redesign of the TC North airspace, the United Kingdom Air Navigation Service Provider (ANSP) NATS proposed environmentally optimizing a number of the SID and STAR designs. One of the SIDs chosen, was the Luton Olney SID, a departure route that runs North from Luton Airport [51].

The Olney SID and the proposed changes to it in the TC-North consultation were taken to form an optimization case study. The environmental impacts of the current and the proposed designs were used as baselines for comparison with solutions proposed by the IDVD-DE method. The aim was to see if the IDVD-DE method could provide better trade-offs between the environmental impacts than those found in the initial study.

The current (D0) and proposed (D1) centrelines for the SIDs are shown in Figure 2. The principle aim of the change to the proposed route was to reduce noise impact by moving traffic away from the densely populated communities of Milton Keynes (MK) and Leighton Buzzard (LB). As can be seen in Figure 2 the route centreline of the current route has been moved such that it no longer passes directly over the population centres. However, to achieve this, the proposed route has been extended, increasing the fuel burn and emissions cost of flying the SID.

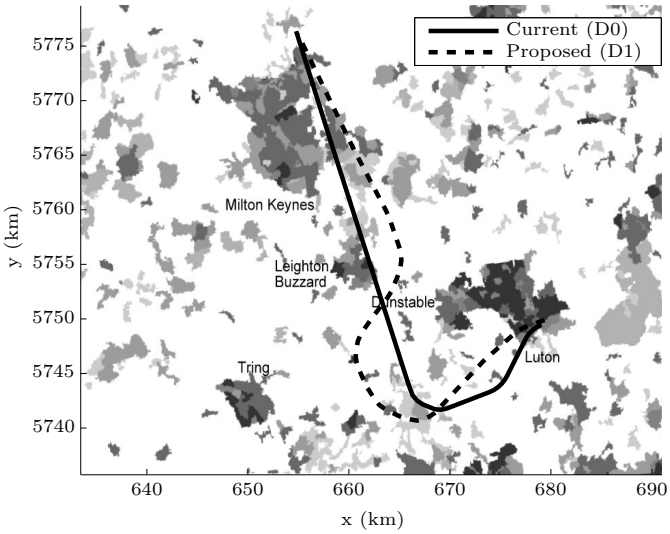

Figure 2: Current and proposed SIDs from the TC North Airspace Change Proposal

The metrics used by NATS in their redesign were fuel burn/CO2 (as calculated by the BADA model) and the number of people overflown. The number of people overflown was used as a surrogate for noise impact. In this case study a single event simulation was conducted using an Airbus A320, the dominant aircraft on the route. To better asses noise impact, this case study has adopted 3 noise measures, L_{Amax} at Milton Keynes (MK), L_{Amax} at Leighton Buzzard (LB) and the total Annoyance Score (17). L_{Amax} was taken as an average L_{Amax} from a grid of points covering each population centre. To balance out the focus on localised noise impact at MK and LB, the Annoyance Score measure was also used to provide an overall community noise impact value. As with the IDVD-DE method, the noise impacts for the baselines were calculated by INM 7 with population data taken from the European Environment Agency database [52]. The fuel burn was calculated using the BADA fuel model.

Table 1, shows the results from the baseline scenarios. As can be seen the proposed SID change achieved its stated goal of reducing the noise impact on large communities. However, this goal was only achieved at the expense of greater fuel burn and greater overall community noise impact as indicated by the fuel burn and Annoyance Score results. To determine if the the IDVD-DE method could propose a better balance of solutions, a multiobjective trajectory optimisation was run.

Scenario	AnoyScore	LAmax MK (dBA)	LAmax LB (dBA)	Fuel (kg)
Current (DO)	$2.6820 \cdot 10^{12}$	43.4	45.7	644
Proposed (D1)	$4.1145 \cdot 10^{12}$	39.1	36.1	677

Table 1: Environmental impact results for baseline procedures

Figure 3 shows the 4 objective Pareto front results produced by the IDVD-DE simulation. The x axis shows the L_{Amax} (dBA) for Milton Keynes, the y axis shows the L_{Amax} (dBA) values for Leighton Buzzard and the z axis shows the Annoyance Score. The 4th axis represents fuel burn, where the size of each data point of the Pareto front reflects the magnitude of the fuel burnt (kg). The range of point sizes and related fuel burn values are shown to the right of the plot. It was decided to constrain the Pareto front solutions to have

an Annoyance Score less than $3 \cdot 10^{12}$. This ensured that solutions identified by the optimisation would at worst only marginally increase the overall community noise impact from the current day noise impact.

The solutions on the Pareto front are clustered according to the extrema solution each point is closest to. The clusters were calculated by measuring the Mahalanobis distance from the extrema solutions to every other solution on the front. Therefore the Pareto front was segmented into 4 individual clusters representing trajectories closest to the lowest fuel burn, Annoyance Score, L_{Amax} at Leighton Buzzard and L_{Amax} at Milton Keynes extrema points respectively.

Figure 4 shows the horizontal paths for the Pareto front trajectories, with the trajectories for each cluster plotted independently. Figures 5, 6 and 7 show the clustered height, speed and thrust profiles for the Pareto front solutions. The average height, speed and thrust profile, independently calculated for each cluster using a moving average, is plotted in black on each chart. Range bars are included to show the mean and the extents of data for each profile set.

Low Fuel Burn Cluster
The low fuel burn cluster represents the trajectories with the lowest fuel burn values. The trajectories in this cluster have a path that includes an early turn to the final fix. In this cluster, there is an early focus on maximising speed at the expense of height. Once 250kts CAS has been reached there is typically a fast climb to the final fix. Although accelerating at low altitudes is expensive in terms of instantaneous fuel burn, it was found that minimising total flight time had a greater effect in minimising total fuel burned.

Low LB LA_{max} Cluster
The low LB LA_{max} cluster represents the trajectories with the lowest maximum noise impact at Leighton Buzzard. The trajectories in this cluster take a long path that circumvents LB and maximises the slant distance between the aircraft and the community. The longer path distances resulted in longer shallower climbs. Thrust cut back occurs early and shallow climbs allow low thrust levels to be maintained until close to the final fix. As all the trajectories in this cluster fly directly over Milton Keynes the peak noise levels at Milton Keynes are consequently high for this clusters trajectories.

Low MK LA_{max} Cluster
The low MK LA_{max} cluster represents the trajectories with the lowest maximum noise impact at Milton Keynes. In this cluster the trajectories maximise the distance from MK by turning as early as possible and emphasising height gain at relatively high thrust levels in order to maximise slant distance between trajectories and Milton Keynes. After the initial climb, gains in speed are emphasised and the cluster has an average speed profile that is close to the average of the profile set.

Low Annoyance Score Cluster
The Low Annoyance Score cluster represents the trajectories that have the lowest Annoyance Score. Trajectories in this cluster exhibit close to average height, speed and thrust profiles. However, the trajectories in the cluster have 2 important properties. They all avoid overflying Leighton Buzzard, passing either to the left or the right of the population centre. They also avoid overflying the Dunstable community adjacent to Luton. A subset of the cluster's trajectories do overfly central Milton Keynes. However, these trajectories more than the others in the cluster, maximise their distance to Leighton Buzzard and Dunstable. This shows that in order to minimise Annoyance Score, the key in this study was to primarily minimise the higher ($>=$ 70 dB(A)) SEL values occurring near takeoff and secondarily, the lower SEL values ($<$ 70 dB(A)) impacting communities further away from the departure runway.

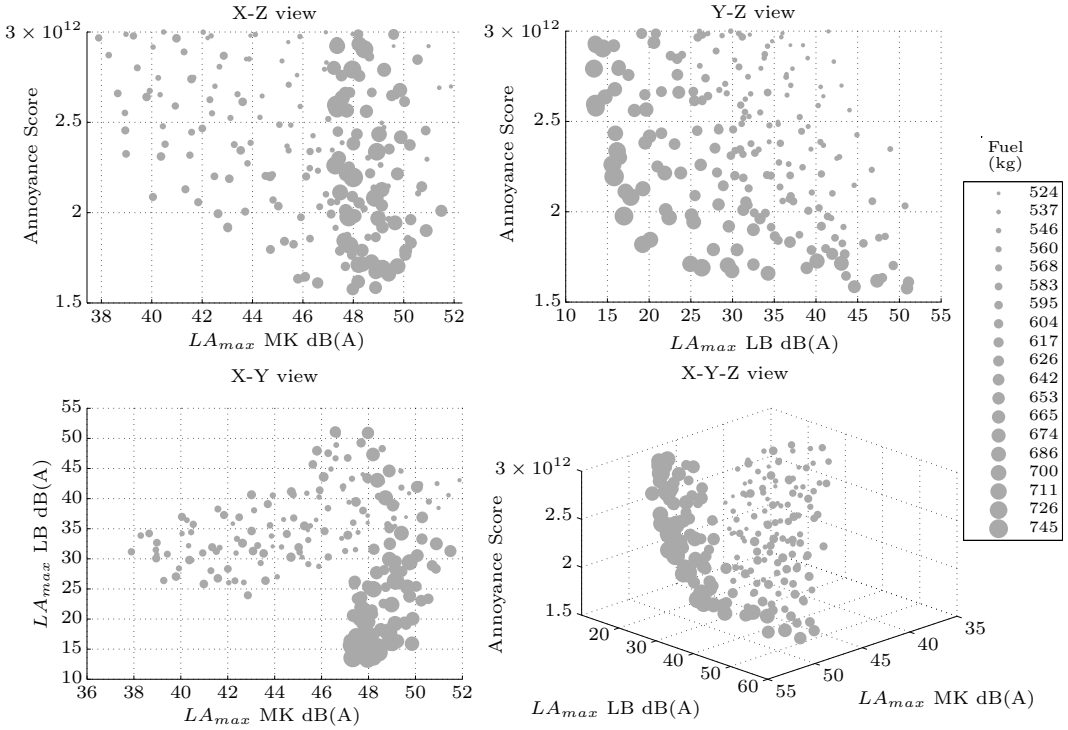

Figure 3: 4 view 4D Pareto front for the Annoyance Score, L_{Amax} MK, L_{Amax} LB and fuel burn measures

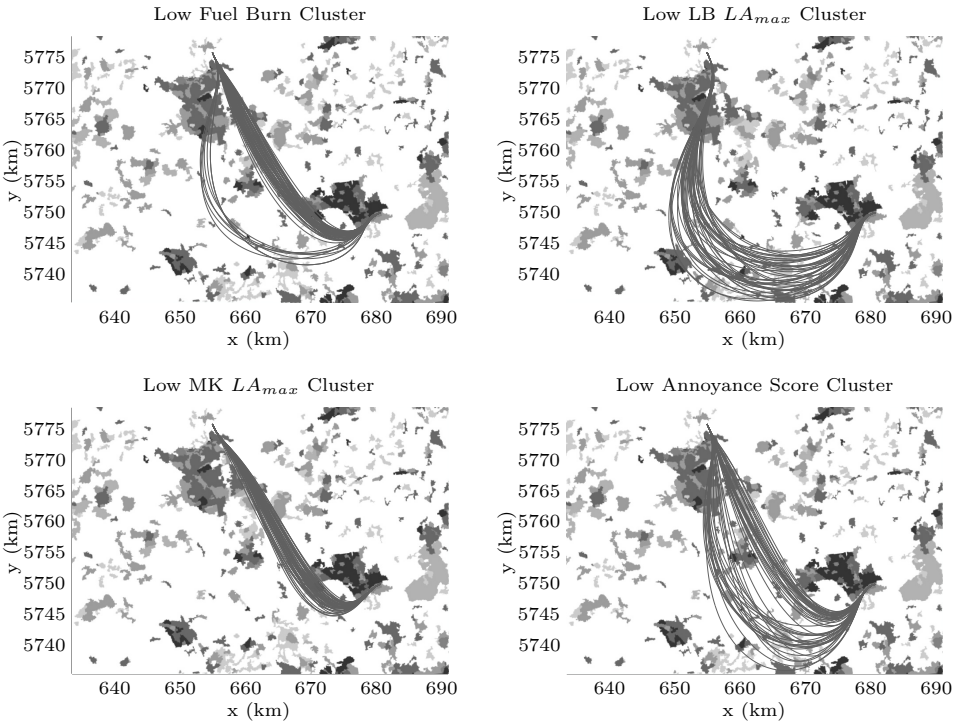

Figure 4: Clustered Pareto front trajectory paths

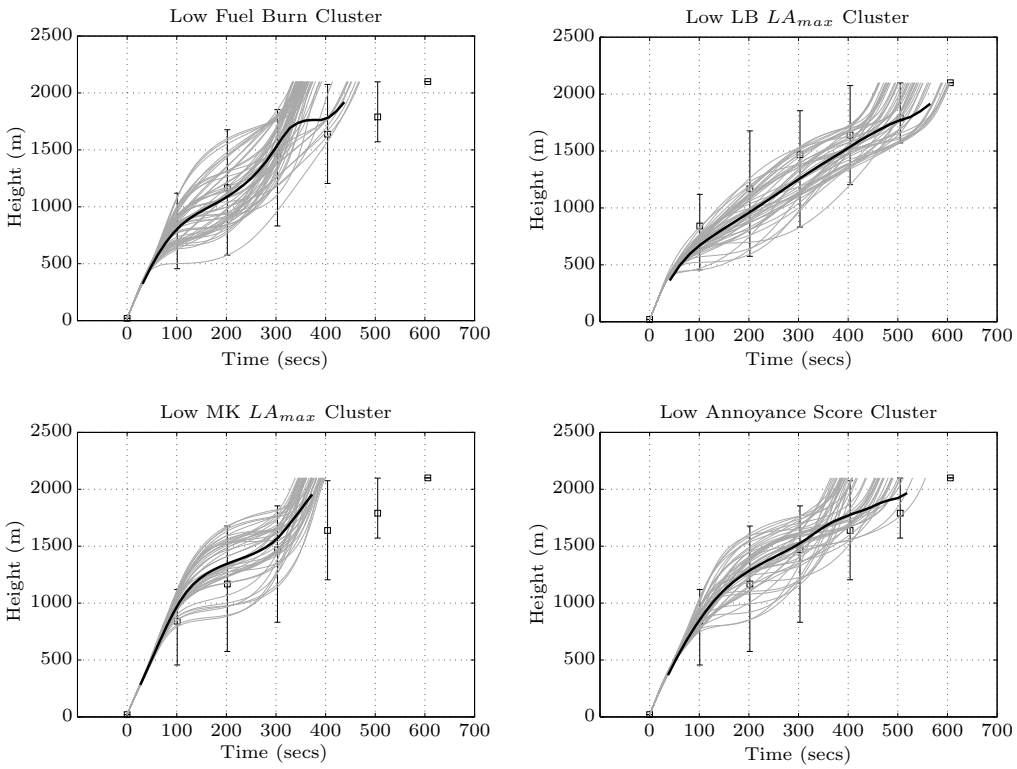

Figure 5: Clustered Pareto front trajectory height profiles

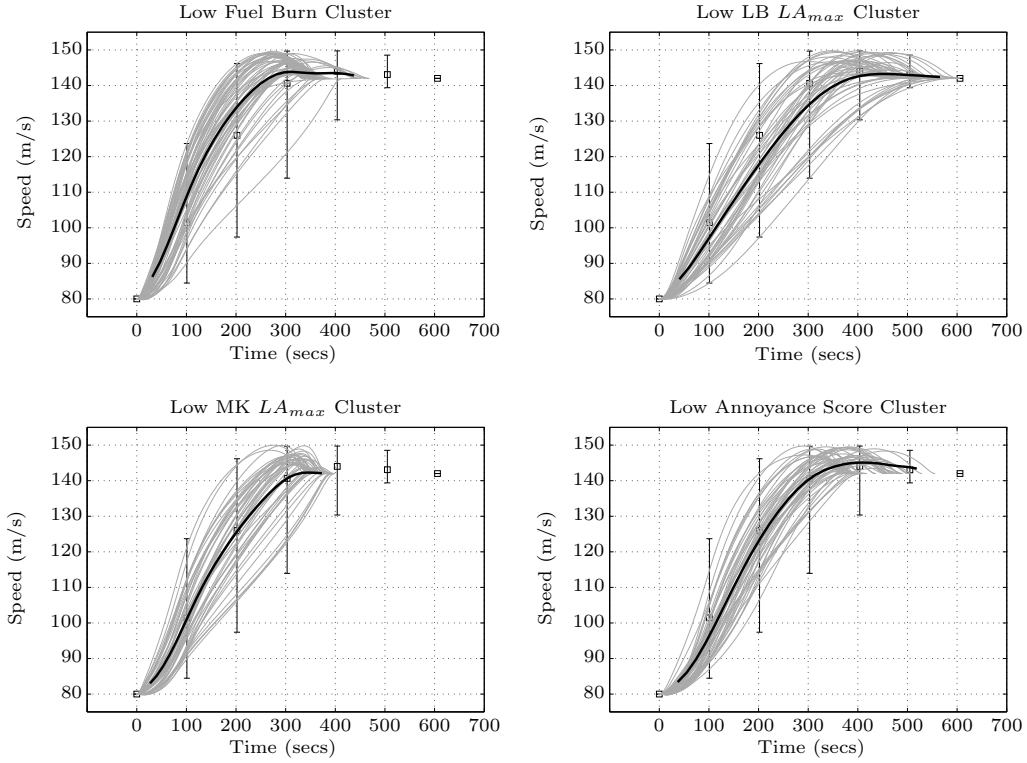

Figure 6: Clustered Pareto front trajectory speed profiles

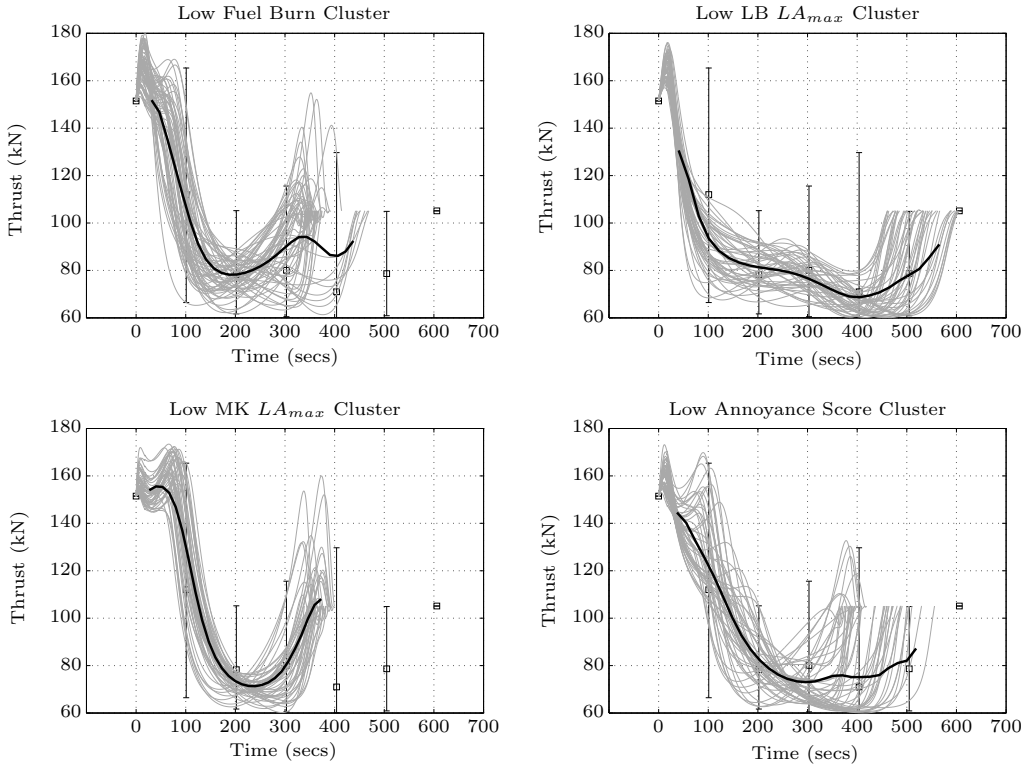

Figure 7: Clustered Pareto front trajectory thrust profiles

6.1 Air Quality

The emissions of NOx, HC and CO were not considered as design objectives in the baseline study but are included here in supplement to the Pareto objectives in Figure 3.

Figure 8 shows the box plots for the trajectory fuel burn and the emissions of NOx, HC and CO clustered as per the Pareto front clustering. The plots show the actual data values plotted over a box showing the mean and a single standard deviation of the mean.

From Figure 8 it can be seen that the lowest fuel burn cluster also had the lowest average emissions values for all of the emissions types. Therefore minimising total trajectory fuel burn clearly has a significant role to play in minimizing emissions.

The clustered results for the emissions HC and CO in Figure 8 exhibit a direct relationship to the clustered total fuel burn values despite the indices of HC and CO both varying inversely to fuel flow. This is due to other factors influencing the emissions results, principally flight time and thrust settings.

CO and HC emissions are formed more prominently at lower combustion efficiencies occurring at lower thrust levels. Therefore, interpolating off the bilinear curves in Figure 1, lower thrust levels and related fuel flows lead to higher emissions indices of HC and CO. Therefore trajectories with the highest summed values of HC and CO are those that have the lowest thrust settings coupled with the longest flight duration times. As flight duration time was also strong indicator of fuel burn, there is a correlation between the clustered fuel burn results and HC/CO emissions results in Figure 8. Cutback thrust and cutback duration were additional factors that impacted the comparisons between clusters having trajectories with similar flight duration times.

The influence of contributing factors other than fuel flow is especially true in the case of the clustered NOx results, which despite there being a linear relationship between EINOx and fuel flow, do not correlate well with the clustered fuel burn values. NOx is formed as a by-product of fuel burn more prominently at higher combustion temperatures related to higher thrust settings. The high thrust levels on climb out for

trajectories in the MK LA_{max} and Annoyance Score clusters result in more NOx values being interpolated off the higher end of the Log-Log Fuel Flow versus EINOx line in Figure 1. This lead to the high summed levels of NOx for these clusters relative to the average flight duration time for trajectories in the clusters.

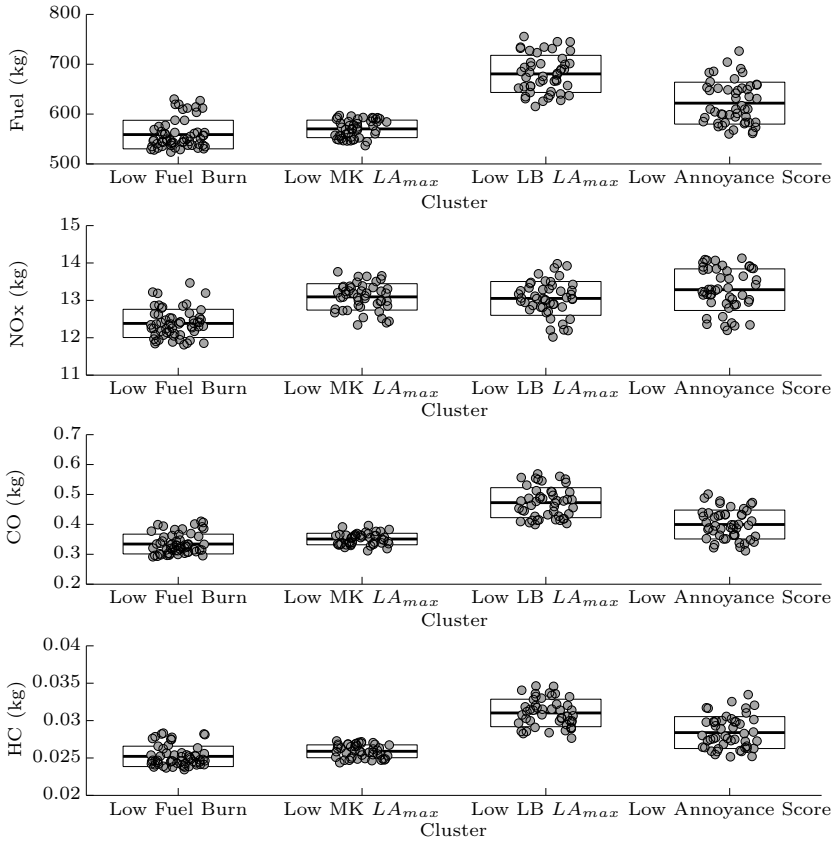

Figure 8: Clustered Pareto front air quality results

6.2 Selection

Using the trajectory and Pareto front information in Figures 3 - 7, it was found that all of the baseline noise results could be achieved at lower fuel burn values. However, there is trade-off between between the Annoyance Score and the peak noise at Milton Keynes making it impossible to have reductions in both measures relative to the baselines.

Figure 9 shows a subset of the Pareto front solutions. The baseline solutions are shown in black. The solutions in the subset were largely identified from the Low MK L_{Amax} cluster, with an extra restriction requiring the Annoyance Score values to be less than or equal to that of the D0 procedure. The subset was chosen as it provided a good balance between the objective values. The region contains points that have Annoyance Scores and fuel burn values less than or equal to the current (D0) procedure, L_{Amax} LB values less than the proposed (D1) procedure, and L_{Amax} MK values less than the D0 route but greater than or equal to those proposed by the D1 route. Therefore the solutions in the selected region offer an improvement over both the existing and proposed routes in 3 of the 4 objectives and offer an improvement in the remaining objective over the current design.

Table 2 shows the mean and standard deviation for fuel burn and air quality emissions for the selected Pareto region. The selected region was identified from the Low MK LA_{max} cluster and has fuel burn, NOx, CO and HC emissions that are equivalent to that cluster. Therefore, it can be seen from Table 2 and Figure 8

that the selected region has NOx, CO and HC values in line or less than the other noise minimising clusters, with only the low fuel burn cluster having better mean values for all emissions.

Metric	Fuel (kg)	NOx (kg)	CO (kg)	HC (kg)
SD	16.5	0.31	0.022	8.66E-04
Mean	576	13.1	0.354	0.0261

Table 2: Mean and standard deviation for fuel burn and air quality emissions for the selected Pareto region

The path, height, speed and thrust profiles for the selected region are shown in Figures 10 and 11. The paths involve a early turn to the final fix with most trajectories passing directly over the Dunstable community. Prior to passing this community, aircraft thrust is held high for an extended period. This allows the aircraft height over Dunstable to be maximised while maintaining a typical speed schedule. Thrust cutback then occurs over the community to levels that are below average relative to the Pareto solutions in Figure 3. The combination of maximised height and low thrust acts to minimise noise on the Dunstable community directly below the route path. Thrust levels as the aircraft subsequently passes Leighton Buzzard, Milton Keynes and intervening smaller communities are maintained low but sufficient for a small continuous acceleration. Once most of Milton Keynes is passed and the target speed for the final fix is reached, higher levels of thrust are reintroduced and the aircraft completes its climb to the final fix.

Figure 9 shows that both the D0 and the selected Pareto front procedures provide lower Annoyance Scores than the D1 procedure. This is because the D1 procedure avoids the major population centres only at the expense of using a longer path that ultimately results a larger number of people in smaller communities being exposed to aircraft noise. The D0 procedure has a lower Annoyance Score than the D1 procedure. The D0 procedure path initially takes aircraft away from Luton and Dunstable but does not do so at the expense of passing through a large number of smaller communities and therefore the D0 procedure minimises the > 70 dB(A) SEL levels that dominate the Annoyance Score results. The earlier turn to the final fix of the D0 procedure also reduces the procedure fuel burn relative to the D1 procedure. For the Pareto solutions in the selected region, Figure 10 shows that all have procedure paths that turn to the final fix before both baselines, providing further reductions in fuel burn results. Unlike the baselines, the Pareto paths pass directly over the densely populated Dunstable community. However, in this case, the vertical trajectories are used to minimise the noise impact on Dunstable in such a way as to achieve lower Annoyance Scores than that achieved by the D0 procedure. In addition, the earlier turn allows the procedure paths to maximise the distance to the right of Leighton Buzzard and Milton Keynes, allowing for the reduction in peak noise values at those communities relative to the D0 procedure and reductions in the peak noise values at Leighton Buzzard relative to the D1 procedure. The subset of Pareto front solutions implicitly define a range of paths and profiles within which the gains in the objective values remain valid. This is useful when defining the procedure extents, and for defining the aircraft and navigation performance required to fly the procedure.

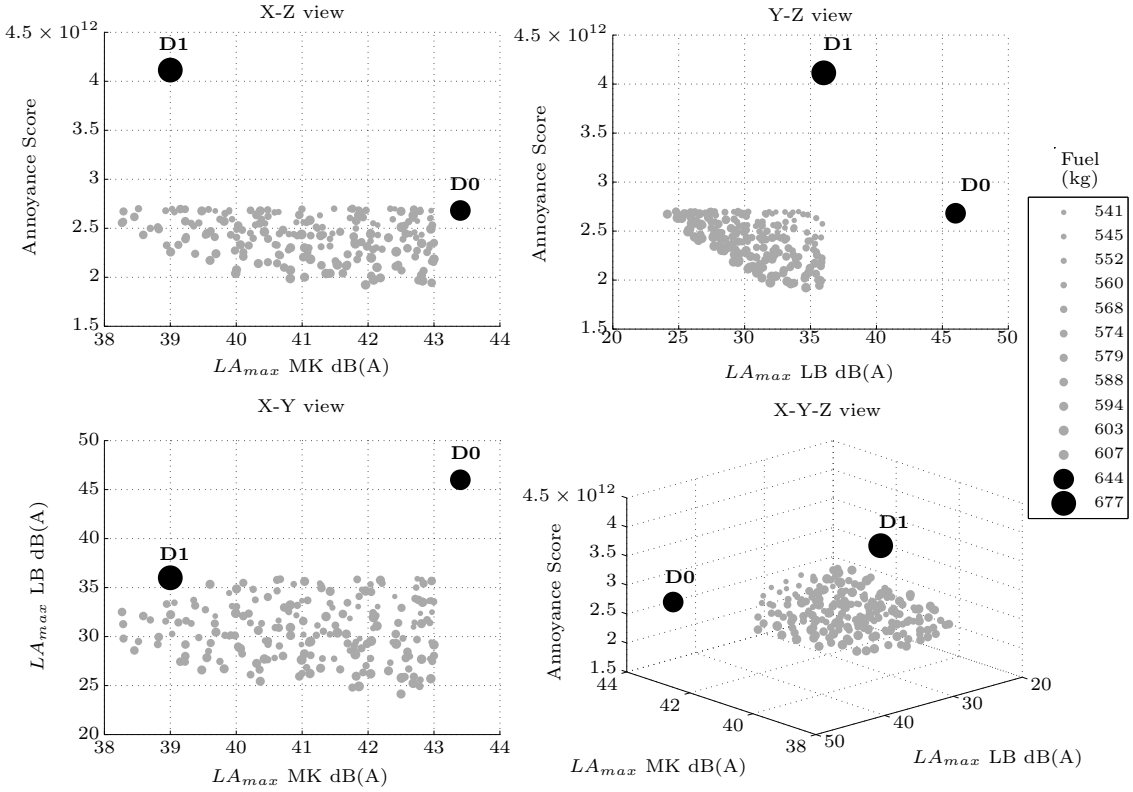

Figure 9: 4 view selected 4D Pareto front with baseline solutions

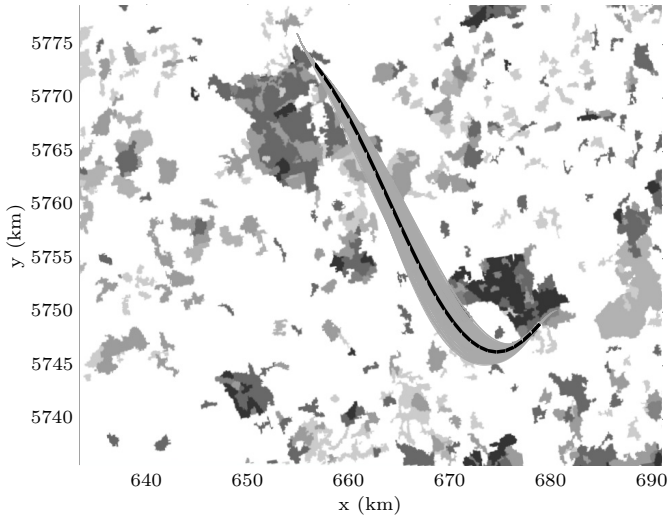

Figure 10: Selected Pareto front trajectory paths

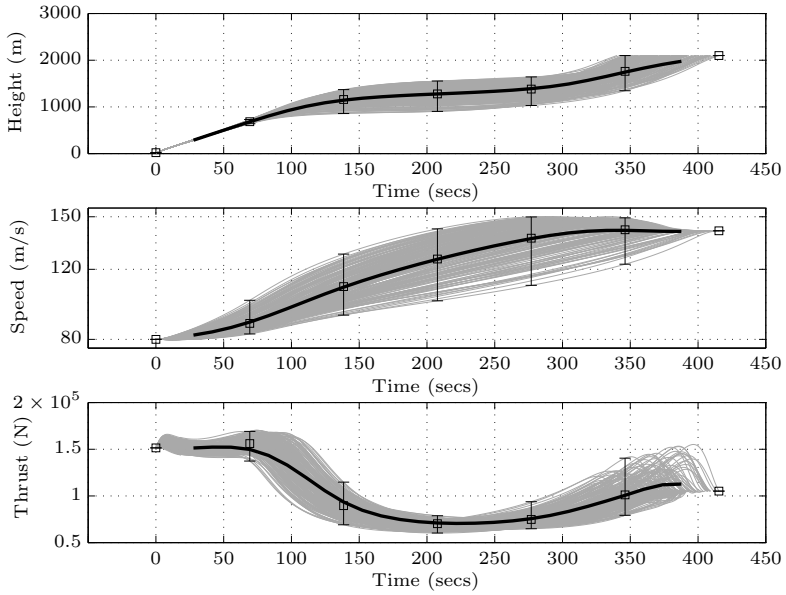

Figure 11: Selected Pareto front trajectory height, speed and thrust profiles from region of interest

6.3 Conversion to Procedure

The Pareto optimal results are intended to provide decision support to route designers considering the placement of departure routes and the definition of related height and speed constraints. The results can be used to provide insight into the trade-offs between the competing environmental objectives. The results were produced with consideration of the dominant aircraft on the route. However SID procedures must be designed to serve a number of different aircraft types with differing navigation equipage that impact the aircraft's ability to fly a given procedure. To ensure compatibility, any recommended trajectory set must be converted to a procedure in line with the procedure design guidance in [8] and validated with further simulations and potentially flight trials. In some instances the multi-use requirement of the procedure may limit the environmental efficiency of the trajectory achievable for any specific aircraft type. In other instances, the procedure constraints may be wide enough to accommodate a wide range of possible trajectories and therefore the emphasis shifts to the aircraft operator to fly the most environmentally balanced trajectory within the procedure constraints.

7 Conclusion

This paper has proposed a methodology intended to produce results that support decision makers seeking to plan environmentally efficient departure procedures. The methodology is intended to be used alongside the 3 ICAO environmental goals of reducing community noise impact, reducing local air quality emissions, and reducing climate changing emissions. In particular, the methodology is designed to support designers in identifying procedures that provide the best trade-offs between these sometimes conflicting environmental objectives.

The paper applied the methodology to a real world case study. The study highlighted the need for a multi-objective optimization method that could be applied to problems with more than two objectives. The method was then used to identify a range of ground paths and related vertical trajectories that, as a group, offered an improvement over both baselines procedures in three of the four objectives and offered an improvement in the final objective over the existing procedure design. Of the metrics used, the Annoyance Score is the least mature and further research is required to determine what constitutes significant changes in Annoyance Score.

The trajectory set identified using the proposed methodology can be used to identify path routing and constraint set information that can be used to inform a procedure design in line with PAN-OPS guidance. The trajectory set can also be used to define the aircraft performance type and navigational performance required to operate the procedure.

References

[1] Airbus, "Delivering the Future: Global Market Forecast 2011-2030," , 2011.

[2] International Civil Aviation Organization, *Environmental Report 2010*, 2010.

[3] Advisory Council Aeronautics Research in Europe, "Strategic Research Agenda. Volume 1," Tech. rep., September 2012.

[4] Advisory Council Aeronautics Research in Europe, "Strategic Research Agenda. Volume 2," Tech. rep., September 2012.

[5] SESAR Joint Undertaking, "SESAR and the Environment," Tech. rep., 2010.

[6] Committee on Aviation Environmental Protection, "Review of Continuous Descent Approach (CDA) Implementation and Associated Benefits," *Working Paper CAEP/7-WP/26*.

[7] Sustainable Aviation, "Sustainable Aviation Noise Road-Map," .

[8] International Civil Aviation Organization, *Aircraft Operations. Volume I: Flight Procedures,*, 2007.

[9] Sourdine Consortium, "Study of Optimisation procedURes for Decreasing the Impact of NoisE (SOURDINE)," *Report D5*.

[10] Visser, H. G. and Wiljnen, R. A., "Optimization of Noise Abatement Departure Trajectories," *Journal of Aircraft*, Vol. 38(4), 2001, pp. 620–627.

[11] Visser, H. G. and Wiljnen, R. A., "Optimization of Noise Abatement Arrival Trajectories," *The Aeronautical Journal*, Vol. 107(1076), 2003, pp. 607–615.

[12] Hargraves, C. and Paris, S., "Direct Trajectory Optimization using Nonlinear Programming and Collocation," in "Astrodynamics 1985," Vol. 1, 1986, pp. 3–12.

[13] Hebly, S. and Visser, H., "Advanced Noise Abatement Departure Procedures: Custom Optimized Departure Profiles," in "AIAA Guidance, Navigation and Control Conference and Exhibit, Honolulu, HI," , 2008.

[14] Houacine, M. and Khardi, S., "Gauss Pseudospectral Method for Less Noise and Fuel Consumption of Aircraft Operations," *Journal of Aircraft*, Vol. 47, No. 6, 2010, pp. 2152–2158.

[15] Soler, M., Olivares, A., and Staffetti, E., "Hybrid Optimal Control Approach to Commercial Aircraft Trajectory Planning," *Journal of Guidance, Control, and Dynamics*, Vol. 33, No. 3, 2010, pp. 985–991.

[16] Herman, A. L. and Conway, B. A., "Direct Optimization using Collocation Based on High-Order Gauss-Lobatto Quadrature Rules," *Journal of Guidance, Control, and Dynamics*, Vol. 19, No. 3, 1996, pp. 592–599.

[17] International Civil Aviation Organization, *Effects of PANS-OPS Noise Abatement Departure Procedures on Noise and Gaseous Emissions*, 2008.

[18] Prats, X., Puig, V., Quevedo, J., and Nejjari, F., "Lexicographic Optimisation for Optimal Departure Aircraft Trajectories," *Aerospace Science and Technology*, Vol. 14, No. 1, 2010, pp. 26–37.

[19] Pervier, H., Nalianda, D., Espi, R., Sethi, V., Pilidis, P., Zammit-Mangion, D., Rogero, J.-M., and Entz, R., "Application of Genetic Algorithm for Preliminary Trajectory Optimization," *SAE International Journal of Aerospace*, Vol. 4, No. 2, 2011, pp. 973–987.

[20] Torres, R., Chaptal, J., Bes, C., and Hiriart-Urruty, J., "Optimal, Environmentally Friendly Departure Procedures for Civil Aircraft," *Journal of Aircraft*, Vol. 48, No. 1, 2011, pp. 11–22.

[21] Fahroo, F. and Ross, I., "Direct Trajectory Optimization by a Chebyshev Pseudospectral Method," in "American Control Conference, 2000. Proceedings of the 2000," IEEE, Vol. 6, 2000, pp. 3860–3864.

[22] Rao, A. V., "A Survey of Numerical Methods for Optimal Control," *Advances in the Astronautical Sciences*, Vol. 135, No. 1, 2009, pp. 497–528.

[23] Hull, D. G., "Conversion of Optimal Control Problems into Parameter Optimization Problems," *Journal of Guidance, Control, and Dynamics*, Vol. 20, No. 1, 1997, pp. 57–60.

[24] Benson, D., Huntington, G., Thorvaldsen, T., and Rao, A., "Direct Trajectory Optimization and Costate Estimation Via an Orthogonal Collocation Method," *Journal of Guidance Control and Dynamics*, Vol. 29, No. 6, 2006, pp. 1435–1440.

[25] Fahroo, F. and Ross, I., "Advances in Pseudospectral Methods for Optimal Control," in "AIAA Guidance, Navigation and Control Conference and Exhibit," , 2008.

[26] Fahroo, F. and Ross, I., "Pseudospectral Methods for Infinite-Horizon Optimal Control Problems," *Journal of Guidance Control and Dynamics*, Vol. 31, No. 4, 2008, pp. 927–936.

[27] Yakimenko, O., "Direct Method for Rapid Prototyping of Near-Optimal Aircraft Trajectories," *AIAA Journal of Guidance, Control, and Dynamics*, Vol. 23, No. 5.

[28] Taranenko, V. T., "Experience on Application of Ritzs, Poincares, and Lyapunovs Methods in Solving of Flight Dynamics Problems," *Air Force Engineering Academy Press Moscow*.

[29] McEnteggart, Q. and Whidborne, J. F., "A Multiobjective Trajectory Optimisation Method for Planning Environmentally Efficient Trajectories," in "Proceedings 2012 UKACC International Conference on Control," , Cardif UK, 2012.

[30] Lai, C. K. and Whidborne, J. F., "Real-time Trajectory Generation for Collision Avoidance with Obstacle Uncertainty," in "AIAA Guidance, Navigation and Control Conference, AIAA 2011-6598," , Portland OR, August 2011.

[31] Nuic, A., "User Manual for the Base of Aircraft Data (BADA) Revision 3.7," Tech. rep., Eurocontrol, 2010.

[32] Glover, W. and Lygeros, J., "A Stochastic Hybrid Model for Air Traffic Control Simulation," in "Hybrid Systems: Computation and Control," Springer, pp. 372–386, 2004.

[33] Figlar, B., Ottl, S., G.and Schwanke, Rodrguez, R. M., Gjestland, T., Ghnemann, A., Harwatt, H., Tight, B. G., M., and Hullah, P., "State of the Art on Tradable Permits, Noise Legislation, Noise Restriction Methods and Noise Modelling," in "EEC MIME WP6.1 SotA," , January 2010.

[34] MIME Consortium, *Final Report of the MIME Project*, 2011.

[35] Granøien, I. L. N. and Gjestland, T., "MIME - Market-based Impact Mitigation for the Environment," in "Proceedings Baltic-Nordic Acoustics Meeting," , Bergen, Norway,2010.

[36] ECAC, "Standard Method of Computing Noise Contours Around Civil Airports ECAC. CEAC Doc. 29," Tech. rep., European Civil Aviation Conference, 2010.

[37] Olmstead, J., Fleming, G., Gulding, J., Roof, C., Gerbi, P., and Rapoza, A., "Integrated Noise Model (INM) Version 7.0 Technical Manual," Tech. rep., Report FAA-AEE-02-01, Office of Environment and Energy, Federal Aviation Administration, 2002.

[38] Baughcum, S. L., Tritz, T. G., Henderson, S. C., and Pickett, D. C., *Scheduled Civil Aircraft Emission Inventories for 1992: Database Development and Analysis*, National Aeronautics and Space Administration, Langley Research Center, 1996.

[39] Storn, R. and Price, K., "Differential Evolution–A Simple and Efficient Heuristic for Global Optimization over Continuous Spaces," *Journal of Global Optimization*, Vol. 11, No. 4, 1997, pp. 341–359.

[40] Price, K., Storn, R., and Lampinen, J., *Differential evolution: a practical approach to global optimization*, Springer-Verlag New York Inc, 2005.

[41] Drury, R. G., "Performance of NLP Algorithms with Inverse Dynamics for Near-Real Time Trajectory Generation," in "AIAA Guidance, Navigation, and Control Conference," , August 2011.

[42] Fonseca, C. M., Fleming, P. J., et al., "Genetic Algorithms for Multiobjective Optimization: FormulationDiscussion and Generalization." in "ICGA," Vol. 93, 1993, pp. 416–423.

[43] Srinivas, N. and Deb, K., "Muiltiobjective Optimization using Nondominated Sorting in Genetic Algorithms," *Evolutionary computation*, Vol. 2, No. 3, 1994, pp. 221–248.

[44] Madavan, N., "Multiobjective Optimization using a Pareto Differential Evolution Approach," in "Evolutionary Computation, 2002. CEC'02. Proceedings of the 2002 Congress on," IEEE, Vol. 2, 2002, pp. 1145–1150.

[45] Lampinen, J., "DEs Selection Rule for Multiobjective Optimization," *Lappeenranta University of Technology, Department of Information Technology, Tech. Rep*, pp. 03–04.

[46] Deb, K., Pratap, A., Agarwal, S., and Meyarivan, T., "A Fast and Elitist Multiobjective Genetic Algorithm: NSGA-II," *Evolutionary Computation, IEEE Transactions on*, Vol. 6, No. 2, 2002, pp. 182–197.

[47] Robic, T. and Filipic, B., "DEMO: Differential Evolution for Multiobjective Optimization," in "Evolutionary Multi-Criterion Optimization," Springer, 2005, pp. 520–533.

[48] Kukkonen, S. and Lampinen, J., "GDE3: The Third Evolution Step of Generalized Differential Evolution," in "Evolutionary Computation, 2005. The 2005 IEEE Congress on," IEEE, Vol. 1, 2005, pp. 443–450.

[49] Deb, K., Thiele, L., Laumanns, M., and Zitzler, E., *Scalable Test Problems for Evolutionary Multiobjective Optimization*, Springer, 2005.

[50] Kukkonen, S. and Deb, K., "A Fast and Effective Method for Pruning of Non-Dominated Solutions in Many-Objective Problems," *Lecture Notes in Computer Science*, Vol. 4193, 2006, pp. 553–562.

[51] NATS, "Consultation Document for the Terminal Control North (TCN) Airspace Change Proposal," *NATS*.

[52] Gallego, F. J., "A Population Density Grid of the European Union," *Population and Environment*, Vol. 31, No. 6, 2010, pp. 460–473.

Multiobjectective environmental departure procedure optimization

McEnteggart, Quintain

2018-04-06

McEnteggart Q, Whidborne JF, Multiobjective environmental departure procedure optimization, Journal of Aircraft, Vol. 55, Issue 3, 2018, pp. 905-917
http://dx.doi.org/10.2514/1.C033132